CACR-96-06

A Fourier-Chebyshev Collocation Method for the Shallow Water Equations Including Shoreline Runup

H. Tuba Özkan-Haller and James T. Kirby
Center for Applied Coastal Research
University of Delaware, Newark, DE 19716

Abstract

A model of the shallow water equations governing wave motions in the nearshore environment is presented. Spatial derivatives contained in these equations are computed using spectral collocation methods. A high-order time integration scheme is used to compute the time evolution of the velocities and water surface elevation given initial conditions. The model domain extends from the shoreline to a desired distance offshore and is periodic in the longshore direction. Properly posed boundary conditions for the governing equations are discussed. A curvilinear moving boundary condition is incorporated at the shoreline to account for wave runup. An absorbing-generating boundary is constructed offshore. The boundary treatments are tested using analytical and numerical results. The model is applied to the prediction of neutral stability boundaries and equilibrium amplitudes of subharmonic edge waves. Numerical results are compared to weakly nonlinear theory and are found to reproduce the theory very well.

1 Introduction

The nonlinear shallow water equations are a set of coupled hyperbolic equations governing many types of processes in the nearshore region. They have been widely employed to model long wave propagation in a variety of cases including tsunami propagation or tidal oscillations. They may also be utilized to model short surface wave propagation, if provision is made to account for dissipation due to wave breaking. Finally, they provide a theoretical basis for modeling

currents and other quasi-steady flows.

Recently, it has been demonstrated that longshore currents induced by obliquely-incident waves breaking on a beach may be unstable to perturbations which induce undulating flow patterns in the longshore direction and time (Oltman-Shay *et al.*, 1989; Bowen and Holman, 1989). The nonlinear shallow water equations provide a good basis for modeling the long-time evolution of these instabilities. Viewed in isolation, these instabilities induce flow perturbations which are primarily horizontal in nature (with vorticity as the primary restoring force), and thus can be studied using rigid-lid models (Allen *et al.*, 1996). However, these motions occur in a complex surf zone environment characterized by a number of additional low-frequency motions, including edge waves and surf beat, which are primarily gravity dominated. The nonlinear shallow water equations provide the leading order approximation of the free surface effects needed to study vorticity and gravity-dominated motions in tandem.

In this paper, we present a numerical treatment of the nonlinear shallow water equations which is specialized to long beaches and to motions which can be assumed to be periodic in the longshore direction. Our aim here is to describe the numerical approach and to verify it in comparison to analytical results for the case of gravity wave motion. Tests involving vorticity waves are not described here, as there are no documented "correct" answers that would serve as a basis for model verification. Instead, results on the evolution of instability waves in the surf zone will be described elsewhere (see Özkan and Kirby (1995) and Özkan-Haller and Kirby (1996) for preliminary results).

First, a model of the nonlinear shallow water equations using Chebyshev collocation in the shore-normal direction in conjunction with Fourier collocation in the shore-parallel direction is presented. The properly posed boundary treatments for these equations are discussed. A curvilinear moving boundary

condition at the shoreline is constructed using an Eulerian model in conjunction with a moving grid. This boundary condition is tested for both one and two-dimensional shoreline runup.

An absorbing-generating boundary condition at the offshore boundary is derived based on the method of characteristics. It is tested for waves leaving the domain at normal or oblique incidence to the artificial offshore boundary.

As we are primarily interested in using the model developed here to study the onset and evolution of instabilities in the surf zone longshore current, the question of whether the model is capable of reproducing unstable behavior in a well understood case is of extreme importance. We thus conclude the paper with an analysis of the growth of subharmonic standing edge waves, which evolve on a long straight beach as a result of an instability of a normally incident (and reflected) long-crested wave. This instability has been studied extensively, and predictions for equilibrium edge wave amplitudes as a function of incident wave conditions and frictional damping rates are available. We show that the present model is capable of reproducing the neutral stability boundaries and equilibrium amplitude predictions for this particular class of motions.

2 Governing Equations

In this study, a two dimensional horizontal model of the non-dispersive continuity and momentum equations is developed. The governing equations, given below, are the nonlinear shallow water equations.

$$D_t + (uD)_x + (vD)_y = 0 \tag{1}$$

$$u_t + uu_x + vu_y = -g\eta_x \tag{2}$$

$$v_t + uv_x + vv_y = -g\eta_y. \tag{3}$$

Here, η is the water surface elevation above the still water level, h is the still water depth, $D = h + \eta$ is the total water depth, u and v are the velocity components in the x and y directions, respectively, where x points offshore and y points in the longshore direction.

The domain in which these equations are solved is shown in Figure 1. It is bounded by a curvilinear moving shoreline at $x = \zeta(y,t)$. This representation of the shoreline boundary imposes the restriction that the shoreline position be single valued in the cross-shore direction x. The kinematic condition for the shoreline dictates that

$$\zeta_t = u^s - v^s \zeta_y, \tag{4}$$

where the superscript s denotes that the variables are evaluated at the shoreline. The physical requirement for a shoreline to exist is

$$D = h + \eta = 0 \quad \text{on } x = \zeta(y,t). \tag{5}$$

Furthermore, the domain is bounded by an open boundary at $x = L_x$. The characteristic horizontal length scale is denoted by L. Periodicity is assumed in the y direction.

Using spectral collocation schemes to determine the spatial derivatives and an explicit time stepping scheme, the most straightforward boundary treatment at, say, $x = L_x$ would be to specify one of the unknowns at the boundary (e.g. u) and update the other two unknowns (v and D) at the boundary using (1), (2) and (3). Although this type of an approach is acceptable when using finite difference methods, it is strongly unstable when spectral collocation methods are used (Gottlieb *et al.*, 1982). The reason is that the use of (1) and (3) for the evolution of v and D is an incorrect extrapolation of the equations to the boundary.

In order to impose the onshore and offshore boundary conditions properly,

we use the method of characteristics and rewrite the governing equations in the unknowns u, v and D in terms of variables that carry information across the onshore and offshore boundaries (herein called the β-characteristic variables) as well as along those boundaries (herein called the γ-characteristic variable). This manipulation is carried out following Abbott (1979).

The governing equations can be written in matrix form as

$$\mathbf{q}_t + \mathbf{A}\mathbf{q}_x + \mathbf{B}\mathbf{q}_y = \mathbf{C}. \tag{6}$$

where

$$\mathbf{q} = \begin{bmatrix} D \\ u \\ v \end{bmatrix}, \quad \mathbf{A} = \begin{bmatrix} u & D & 0 \\ g & u & 0 \\ 0 & 0 & u \end{bmatrix}, \quad \mathbf{B} = \begin{bmatrix} v & 0 & D \\ 0 & v & 0 \\ g & 0 & v \end{bmatrix}, \quad \text{and} \quad \mathbf{C} = \begin{bmatrix} 0 \\ gh_x \\ gh_y \end{bmatrix}. \tag{7}$$

The eigenvector matrix $\mathbf{P}$ of the matrix $\mathbf{A}$ is given by

$$\mathbf{P} = \begin{bmatrix} -\frac{1}{2}\sqrt{D/g} & \frac{1}{2}\sqrt{D/g} & 0 \\ \frac{1}{2} & \frac{1}{2} & 0 \\ 0 & 0 & 1 \end{bmatrix}. \tag{8}$$

Premultiplying (6) by the inverse matrix $\mathbf{P^{-1}}$ gives

$$\mathbf{P}^{-1}\mathbf{q}_t + \left(\mathbf{P}^{-1}\mathbf{A}\mathbf{P}\right)\mathbf{P}^{-1}\mathbf{q}_x + \left(\mathbf{P}^{-1}\mathbf{B}\mathbf{P}\right)\mathbf{P}^{-1}\mathbf{q}_y = \mathbf{P}^{-1}\mathbf{C}. \tag{9}$$

Algebraic manipulation of this equation results in

$$\mathbf{w}_t + \mathbf{A}'\mathbf{w}_x + \mathbf{B}'\mathbf{w}_y = \mathbf{C}'. \tag{10}$$

where

$$\mathbf{A}' = \begin{bmatrix} u - \sqrt{gD} & 0 & 0 \\ 0 & u + \sqrt{gD} & 0 \\ 0 & 0 & u \end{bmatrix}, \quad \mathbf{B}' = \begin{bmatrix} v & 0 & -\sqrt{gD} \\ 0 & v & \sqrt{gD} \\ -\frac{1}{2}\sqrt{gD} & \frac{1}{2}\sqrt{gD} & v \end{bmatrix},$$

$$\text{and} \quad \mathbf{C}' = \begin{bmatrix} gh_x \\ gh_x \\ gh_y \end{bmatrix}. \tag{11}$$

The unknown vector $\mathbf{w}$ is defined by

$$\mathbf{w} \equiv \begin{bmatrix} u - 2\sqrt{gD} \\ u + 2\sqrt{gD} \\ v \end{bmatrix} \equiv \begin{bmatrix} \beta^- \\ \beta^+ \\ \gamma \end{bmatrix}. \tag{12}$$

The three equations can now be written as

$$\beta_t^- + (u - c)\beta_x^- + v\beta_y^- - c\gamma_y = 2c_0 c_{0x} \tag{13}$$

$$\beta_t^+ + (u + c)\beta_x^+ + v\beta_y^+ + c\gamma_y = 2c_0 c_{0x} \tag{14}$$

$$\gamma_t + u\gamma_x + v\gamma_y = -g\eta_y. \tag{15}$$

Here, c is the nonlinear shallow water wave speed $\sqrt{gD} = \sqrt{g(h+\eta)}$ and c_0 is the linear shallow water wave speed $\sqrt{gh}$. Note that, in the absence of longshore variability, the above equations reduce to uncoupled one-way wave equations. As desired, the variables β^- and β^+ carry information across the onshore and offshore boundaries whereas the variable γ carries information along those boundaries.

Note that the equation governing $\beta^+ = u + 2c$ ($\beta^- = u - 2c$) carries information in the $+x$ ($-x$) direction and is therefore valid everywhere inside the domain and on the right (left) boundary point but not on the left (right) boundary point. The equation governing the evolution of the glancing variable $\gamma = v$ is valid everywhere in the domain including the boundary points.

In order to impose the boundary condition at $x = L_x$ properly, the incoming β variable β^- has to be specified, while the outgoing β variable β^+ and the glancing variable γ can be computed using (14) and (15), respectively. The simplest boundary that can be constructed in this manner at, say, $x = L_x$ is a fully reflective wall boundary, where β^+ and γ are calculated using (14) and (15) and β^- is specified as $\beta^- = -\beta^+$. Numerical calculations using this condition lead to stable solutions.

3 Treatment of Moving Shoreline

Gravity driven motions in the nearshore region have significant shoreline runup associated with them. The most commonly used techniques to model shoreline runup are Eulerian models with fixed numerical grids or meshes. Examples of the implementation of such methods can be found in studies of solitary wave and tsunami runup such as Liu *et al.* (1995). In these methods the shoreline is defined as the interface between wet and dry cells; therefore, it is usually defined within the accuracy of the grid size. The shoreline is advanced or retreated in discrete steps. The amount of movement is dictated by the volume flux at the last wet point. These methods are fairly straightforward to implement. However, the impulsive filling of a cell with fluid can lead to numerical problems or time step constraints unless treated carefully. Also, an *a priori* estimate of the maximum runup needs to be available in order to keep the domain large enough to accommodate it.

Lagrangian methods are very well suited for the treatment of moving boundaries. In these methods, the fluid is represented as a large number of fluid particles. Tracking the position of a particle at the shoreline is in general no more difficult than tracking a particle in the interior of the fluid. Examples of computations for solitary wave runup using Lagrangian methods are presented by Pedersen and Gjevik (1983) and Zelt and Raichlen (1990). However, Lagrangian methods employed in regions with a net streaming velocity (such as the longshore current in the surf zone) may require frequent regridding, since the computational grid would tend to be advected and sheared by the steady flow.

Eulerian models with deforming grids are less frequently used in association with long wave runup. Lynch and Gray (1980) and Gopalakrishnan and Tung (1983) reported techniques whereby moving boundaries can be treated by finite

element Eulerian models. They involve moving grids where one boundary of the grid tracks the position of the shoreline, and are more difficult to implement than methods involving a fixed grid. However, they do not exhibit the problems associated with grid draining and filling in fixed grid models, and would not experience the difficulties associated with steady flows in a purely Lagrangian model. Therefore, we have chosen to develop an Eulerian model with a moving grid for application to the surf zone in the present study.

The problem at hand consists of solving a set of well-known governing equations (13), (14) and (15) in a complicated physical domain bounded by one curvilinear moving boundary defined by (4) and (5) and three stationary boundaries. The challenge of modeling the moving boundary can be overcome by mapping the variable size domain onto a fixed domain. Such a transformation will lead to a grid that follows the shoreline with one grid boundary and will introduce additional terms into the governing equation.

The coordinate transformation from the physical variables $x \in [\zeta(y,t), L_x]$ and $y \in [0, L_y]$ to the intermediate variables $\phi \in [0, L_x]$ and $\psi \in [0, L_y]$ used here is given by

$$x = \phi + \zeta(y,t)e^{-\alpha\phi^2}, \qquad y = \psi. \tag{16}$$

A stationary orthogonal grid in the (ϕ, ψ) domain corresponds to a physical grid that is following the shoreline (see Figure 2). The movement of the grid lines is damped out exponentially with offshore distance so that the grid is almost stationary at a certain distance offshore. This distance is dictated by the value of the parameter α. As a result of the transformation, the derivatives in the governing equations are altered, resulting in a few additional terms. The derivatives in the governing equations now become

$$(\ )_t|_x \;=\; (\ )_t|_\phi + (\ )_\phi \phi_t$$

$$
\begin{aligned}
(\,)_x &= (\,)_\phi \phi_x \\
(\,)_y &= (\,)_\psi + (\,)_\phi \phi_y,
\end{aligned} \tag{17}
$$

where $\phi(x, y, t)$ is given by (16) and $(\,)_t|_x$ and $(\,)_t|_\phi$ denote time derivatives in a reference frame where x and ϕ are fixed, respectively.

The intermediate grid in the variables $\phi \in [0, L_x]$ and $\psi \in [0, L_y]$ obtained above is next mapped onto a computational grid in the variables $s \in [-1, 1]$ and $r \in [0, L_y]$ (see Figure 3). The coordinate transformation

$$
\phi = L\frac{1+s}{s_0 - s}, \qquad \psi = r \tag{18}
$$

is used. The value of the parameter s_0 is dictated by the location of the offshore boundary. If the offshore boundary is located at infinity s_0 equals unity. In this case a physical domain in the shape of a semi-infinite strip is modeled while the computations are carried out in a box-shaped domain. For a finite offshore width $s_0 > 1$.

As a result of this second transformation the derivatives in the governing equation are further modified and become,

$$
\begin{aligned}
(\,)_t|_x &= (\,)_t|_s + (\,)_s s_\phi \phi_t \\
(\,)_x &= (\,)_s s_\phi \phi_x \\
(\,)_y &= (\,)_r + (\,)_s s_\phi \phi_y,
\end{aligned} \tag{19}
$$

where $\phi(x, y, t)$ and $s(\phi)$ are given by (16) and (18), respectively. Here, $(\,)_t|_s$ denotes time derivatives at fixed values of s.

As a result of the two coordinate transformations the governing equations now read

$$
\beta_t^- + [s_t + s_x(u - c) + s_y v]\,\beta_s^- + v\beta_r^- - c\gamma_r - s_y c\gamma_s = 2s_x c_0 c_{0_s} \tag{20}
$$

$$
\beta_t^+ + [s_t + s_x(u + c) + s_y v]\,\beta_s^+ + v\beta_r^+ + c\gamma_r + s_y c\gamma_s = 2s_x c_0 c_{0_s} \tag{21}
$$

$$
\gamma_t + [s_t + s_x u + s_y v]\,\gamma_s + v\gamma_r = -g\eta_r - g s_y \eta_s. \tag{22}
$$

At the shoreline $c = \sqrt{gD} = 0$, and the equations in the β-variables collapse into one redundant equation and no information about the values of the β-variables can be deduced. However, the velocity at the shoreline can be determined using the x-momentum equation

$$u_t^s + \left[s_t + s_x u^s + s_y v^s\right] u_s^s + v u_r^s = -g s_x \eta_s^s, \tag{23}$$

where the superscript s denotes that the variables are evaluated at the shoreline. After applying the two coordinate transformations the kinematic condition (4) reads

$$\zeta_t = u^s - v^s \zeta_r. \tag{24}$$

The physical requirement (5) for a shoreline to exist becomes

$$D = h + \eta = 0 \quad \text{on } s = -1. \tag{25}$$

The evolution of the wave field is calculated by time stepping (20), (21) and (22) along with (23) and (24) while imposing the condition stated in (25) and an offshore boundary condition to be discussed next.

In the following sections, it will be shown that this boundary treatment compares favorably to analytical and other numerical results. However, in some situations, especially when steep waves are involved, it causes grid points to run up the shore to form a thin film of water on the beach. As a result grid points are lost to the beach and the resolution of the solution is decreased. Therefore, it is necessary to prevent the occurrence of a thin film which is evidenced by more than one grid point with $D < D_{thresh}$ associated with them. The parameter D_{thresh} is a threshold value appropriate for the application. If the occurrence of a thin film is detected, the shoreline position is redefined as the average of the positions of the most seaward point with $D < D_{thresh}$ and the next offshore point with $D > D_{thresh}$. The row at the longshore positions where the thin film was detected is then regridded.

4 Offshore Absorbing-Generating Boundary

An absorbing-generating boundary condition needs to be specified at the offshore boundary to simultaneously allow waves to exit the domain of interest with minimum reflection as well as specify incoming waves at the offshore boundary. The logic of the absorbing-generating boundary condition can be best understood when the problem is reduced to a one dimensional case. The extension to the two dimensional problem follows in a straightforward manner.

4.1 One dimensional problem

In one dimension, the governing equations at the offshore boundary $x = L_x$ reduce to

$$\beta_t^- + (u - c)\beta_x^- = 2c_0 c_{0x} \tag{26}$$

$$\beta_t^+ + (u + c)\beta_x^+ = 2c_0 c_{0x}, \tag{27}$$

which are uncoupled one-way wave equations. The characteristic variables are given by $\beta^- = u - 2c$ traveling in the $-x$ direction and $\beta^+ = u + 2c$ traveling in the $+x$ direction.

If an outgoing wave exists in the absence of an incoming wave, the incoming characteristic will carry no information and will reduce to $\beta^- = u - 2c = -2c_0$. Therefore, the particle velocity associated with the outgoing wave is $U_{out} = 2c_{out} - 2c_0$, where $c_{out} = \sqrt{g(h + \eta_{out})}$. In this case the boundary condition at the offshore boundary $x = L_x$ would be constructed by computing the outgoing characteristic β^+ using (27) and specifying the incoming characteristic β^- as $-2c_0$.

In turn, if an incoming wave exists in the absence of an outgoing wave, the outgoing characteristic will carry no information and will reduce to $\beta^+ = u + 2c = 2c_0$. The particle velocity associated with the incoming wave is then $U_{in} =$

$-2c_{in}+2c_0$, where $c_{in} := \sqrt{g(h+\eta_{in})}$. The specification of the boundary condition is again straightforward; β^+ can be computed using the governing equation and β^- has to be specified as the incoming wave.

Assuming that the incoming and outgoing waves exist simultaneously but that their particle velocities are independent of each other the observed velocity at the boundary is $u = U_{in} + U_{out} = 2(c_{out} - c_{in})$ and the total water surface elevation is $\eta = \eta_{in} + \eta_{out}$. This assumption is equivalent to superimposing the incoming and outgoing waves at the boundary. However, this superposition does not imply a linearization of the problem at the boundary since the velocities associated with the waves are calculated using the nonlinear equations. As a result, the interactions between the incoming and outgoing waves are neglected while the self-interactions of these waves are included.

4.2 Two dimensional problem

The extension of the above ideas to the two dimensional case has previously been presented by Verboom *et al.* (1984) for the case of wave absorption for a viscous fluid. A similar technique has been used by Van Dongeren *et al.* (1994) for simultaneous absorption-generation in the context of long wave propagation.

The technique involves defining the particle velocities of the incoming and outgoing waves as U_{in} and U_{out}, respectively, along with their components in the x direction u_{in} and u_{out} and their components in the y direction v_{in} and v_{out} (see Figure 4). Known quantities at the offshore boundary $x = L_x$ are variables associated with the known incoming wave u_{in}, v_{in} and η_{in} as well variables determined from the governing equations $v = v_{in} + v_{out}$ and $\beta^+ = u + 2c$ where $u = (u_{in} + u_{out})$ and $c = \sqrt{g(h + \eta_{in} + \eta_{out})}$. The unknowns are the x-component of the outgoing wave particle velocity u_{out} and its propagation speed c_{out}, which is defined above.

The total celerity c can be rewritten as

$$c^2 = c_{in}^2 + c_{out}^2 - c_0^2. \tag{28}$$

Since $\beta^+ = u + 2c$ is known, we can write,

$$4c_{out}^2 = \left(\beta^+ - u\right)^2 - 4c_{in}^2 + 4c_0^2. \tag{29}$$

¿From the discussion about the one dimensional problem, we can deduce that in the absence of any interaction with the incoming wave, the particle velocity of the outgoing wave in the propagation direction is given by,

$$U_{out} = 2c_{out} - 2c_0 \tag{30}$$

or,

$$4c_{out}^2 = \left(U_{out} + 2c_0\right)^2. \tag{31}$$

Equating the right hand sides of (29) and (31), rearranging and using $u = (u_{in} + u_{out})$ gives,

$$u_{out} = (\beta^+ - u_{in}) - \left[U_{out}^2 + 4U_{out}c_0 + 4c_{in}^2\right]^{1/2}. \tag{32}$$

Using geometrical arguments (see Figure 4), it can be stated that $U_{out}^2 = u_{out}^2 + v_{out}^2$. Substituting the expression for u_{out} given in (32) and rearranging gives

$$dU_{out}^2 + eU_{out} + f = 0, \tag{33}$$

where,

$$\begin{aligned} d &= (\beta^+ - u_{in} - 2c_0)(\beta^+ - u_{in} + 2c_0) \\ e &= 2c_0\left[(\beta^+ - u_{in})^2 - v_{out}^2 - 4c_{in}^2\right] \\ f &= -\frac{1}{4}\left[(\beta^+ - u_{in} - 2c_{in})^2 + v_{out}^2\right]\left[(\beta^+ - u_{in} + 2c_{in})^2 + v_{out}^2\right]. \end{aligned} \tag{34}$$

Now, the unknown particle velocity U_{out} can be found to be

$$U_{out} = \begin{cases} \left(-e \pm \sqrt{e^2 - 4df}\right)/(2d) & \text{for } d \neq 0 \\ -f/e & \text{for } d = 0 \end{cases} \tag{35}$$

Therefore,

$$\begin{aligned} u_{out} &= \mathrm{sgn}(U_{out})\sqrt{U_{out}^2 - v_{out}^2} \\ c_{out} &= c_0 + \frac{1}{2}U_{out}. \end{aligned} \tag{36}$$

The incoming β-variable can be specified as

$$\beta^- = (u_{in} + u_{out}) - 2c, \tag{37}$$

where c is given by (28).

5 Numerical Solution Method

Traditionally, the most straightforward method to solve the shallow water equations has involved making finite difference approximations of spatial derivatives in conjunction with an explicit or implicit time stepping scheme. The accuracy of such methods is limited due to truncation errors associated with the difference approximations. These errors usually arise in the form of dispersion or dissipation errors. More recently, spectral and pseudospectral methods have become more popular. A wide variety of spectral schemes exist and are reviewed in Canuto *et al.* (1987) and Boyd (1988). A recent application of spectral schemes to water wave propagation problems has been performed by Panchang and Kopriva (1989) who used a Chebyshev collocation method to analyze short wave propagation over complicated bathymetry. In addition, Falqués and Iranzo (1992) applied spectral collocation methods to the linear shallow water equations. Dalrymple *et al.* (1994) compared several spectral methods in the context of forward propagating water waves. When compared to finite difference methods, spectral methods give more accurate approximations for spatial derivatives, as they have no truncation errors and therefore lead to more accurate solutions with less dispersion and dissipation errors. Furthermore, they can be tailored to suit the

motions of interest since basis functions for the spectral derivatives can be chosen to naturally satisfy the boundary conditions and variable grid spacing can easily be incorporated to achieve high resolution where steep solutions are expected. In this manner a solution of the desired accuracy can be achieved with far less spatial points and therefore, less computational time than with finite difference schemes. Since these are desired features of the model, spectral collocation schemes are employed herein for the computation of the spatial derivatives.

Given initial conditions for the water surface elevation η and the velocities u and v, the governing equations given in (20), (21) and (22) are integrated in time using an explicit third order Adams-Bashforth scheme. The governing equations can be written in the form

$$\beta_t^- = F_1(\eta, u, v) \tag{38}$$

$$\beta_t^+ = F_2(\eta, u, v) \tag{39}$$

$$\gamma_t = F_3(\eta, u, v). \tag{40}$$

The definitions for $F_1(\eta, u, v)$, $F_2(\eta, u, v)$ and $F_3(\eta, u, v)$ contain spatial derivatives of their arguments and can be obtained by comparing (38) through (40) to (20) through (22).

The third order Adams-Bashforth scheme is given by

$$\left(\beta^-\right)^{n+1} = \left(\beta^-\right)^n + \frac{\Delta t}{12}\left[23F_1^n - 16F_1^{n-1} + 5F_1^{n-2}\right] \tag{41}$$

$$\left(\beta^+\right)^{n+1} = \left(\beta^+\right)^n + \frac{\Delta t}{12}\left[23F_2^n - 16F_2^{n-1} + 5F_2^{n-2}\right] \tag{42}$$

$$\gamma^{n+1} = \gamma^n + \frac{\Delta t}{12}\left[23F_3^n - 16F_3^{n-1} + 5F_3^{n-2}\right]. \tag{43}$$

The superscripts denote the time level at which the terms are evaluated with n being the present, known time level.

The spatial derivatives in the right hand side of (38),(39) and (40) are computed using spectral collocation. The advantage to using spectral derivatives is

the accuracy that can be achieved. For smooth solutions, the error asymptotically decays faster than any polynomial order (Canuto *et al.*, 1987) compared to a low fixed polynomial order for finite difference derivatives. Therefore, a desired accuracy can usually be achieved with spectral methods using far less spatial points than for finite difference schemes. In addition, spectral methods introduce no dispersion errors.

In order to apply spectral methods to the problem at hand, the domain of interest is discretized into an $(NX+1) \times (NY+1)$ point mesh. The collocation points in the offshore direction s are chosen as the reversed Gauss-Lobatto points given by $s_i = -\cos(\pi i/NX)$ $(i = 0, \ldots, NX)$. This choice ensures that the grid points in the physical domain are concentrated close to the shoreline. Using these collocation points, the Chebyshev collocation calculations can also be carried out using efficient Fast Fourier Transform (FFT) routines.

The collocation points in the longshore direction r are chosen to be equally spaced so that $r_j = j\Delta y$ $(j = 0, \ldots, NY)$. Fourier collocation is applied in this direction since the Fourier basis functions naturally satisfy the periodicity boundary condition imposed in the longshore direction.

Let Q represent one of the variables β^-, β^+ or γ at a certain time level. Using Fourier collocation for the r direction derivatives in the governing equations and a Chebyshev collocation method for the s direction derivatives Q will be approximated by

$$Q(s,r) \approx Q_p(s,r) = \sum_{m=0}^{NY} \sum_{n=0}^{NX} a_{nm} T_n(s) e^{imkr} \tag{44}$$

where $T_n(s), n = 0, 1, \ldots$ are Chebyshev polynomials of the first kind and are given by

$$T_n(s) = \cos n\theta, \qquad \theta = \arccos s. \tag{45}$$

Approximations to the derivatives in the longshore direction r are computed

by differentiating (44) with respect to r. Rewriting the equation gives,

$$Q_p(s,r) = \sum_{m=0}^{NY} A_m(s) e^{imkr}, \text{ where } A_m(s) = \sum_{n=0}^{NX} a_{nm} T_n(s). \tag{46}$$

The function $A_m(s)$ is known since it is the Fourier transform of Q_p in r at a fixed s location. Differentiating the above equation yields

$$(Q_p(s,r))_r = \sum_{m=0}^{NY} A'_m(s) e^{imkr}, \text{ where } A'_m(s) = imkA_m(s) \tag{47}$$

Thus, inverse Fourier transforming $A'_m(s)$ gives the desired spatial derivative. Note that the derivative of Q_p along an x line is a function of the values of Q_p at all the y locations, hence the derivative has a global character. Furthermore, the procedure defines the values of the derivatives at all mesh points, no special procedure is required to evaluate derivatives at the boundaries.

The derivatives in the s direction are computed using Chebyshev collocation. The procedure is much like that described above for Fourier collocation. Rewriting (44) yields

$$Q_p(s,r) = \sum_{n=0}^{NX} B_n(r) T_n(s), \text{ where } B_n(r) = \sum_{m=0}^{NY} a_{nm} e^{imkr}. \tag{48}$$

The function $B_n(r)$ is known as the Chebyshev transform of Q_p in s at a fixed r location. Differentiating with respect to s gives

$$(Q_p(s,r))_s = \sum_{n=0}^{NX} B'_n(r) T_n(s). \tag{49}$$

Using the definition for the Chebyshev polynomials given in (45) and the trigonometric identity $2\sin\theta\cos n\theta = \sin(n+1)\theta - \sin(n-1)\theta$, the coefficients $B'_n(r)$ can be computed in decreasing order by the recurrence relation

$$c_n B'_n(r) = B'_{n+2}(r) + 2(n+1)B_{n+1}(r), \tag{50}$$

where

$$c_n = \begin{cases} 2 & \text{if } n = 0 \\ 1 & \text{if } n \geq 1 \end{cases} \quad \text{and} \quad B'_n(r) = 0 \quad \text{for } n \geq NX \tag{51}$$

Once again, no special boundary treatment is needed. Both methods of differentiation are described in detail by Canuto *et al.* (1987).

A type of instability in the time integration of nonlinear systems is caused by the process known as aliasing. The onset of the aliasing instability is characterized by the excitement of waves at the limit of the resolution. In the simulations shown here, a solution smoothing technique involving a high order filter developed by Shapiro (1970) is used to prevent the spurious growth of the shortest waves that can be resolved and avoid aliasing. The filter effectively eliminates waves at twice the grid spacing but applies only minimum damping to all longer waves while preserving the relative phases of waves of any wavelength.

6 Test Cases

In this section, the accuracy of the boundary treatments is verified using several test cases. First the shoreline boundary condition is tested for one dimensional as well as two dimensional runup. The offshore boundary is tested for waves leaving the domain of interest at normal incidence or at an angle to the offshore direction.

6.1 Shoreline Boundary

1D Runup

An analytical solution for single wave runup on a sloping beach by Carrier and Greenspan (1958) is used to verify the accuracy of the shoreline treatment. This example corresponds to the physical problem in which the water level at the shoreline is depressed, the fluid is held motionless and then released. The shoreline water level climbs to a position higher than the still water level, and then slowly settles back to it.

The initial water surface elevation η as a function of offshore distance x can be expressed in parametric form as

$$\begin{aligned} \eta &= \epsilon m L \left[1 - \frac{5}{2} \frac{a^3}{(a^2+\xi^2)^{3/2}} + \frac{3}{2} \frac{a^5}{(a^2+\xi^2)^{5/2}} \right] \\ x &= -\frac{L}{16}\xi^2 + \epsilon m L \left[1 - \frac{5}{2} \frac{a^3}{(a^2+\xi^2)^{3/2}} + \frac{3}{2} \frac{a^5}{(a^2+\xi^2)^{5/2}} \right] \end{aligned} \tag{52}$$

for $\xi > 0$, where $a = 1.5(1 + 0.9\epsilon)^{1/2}$. The parameter ϵ is the maximum nondimensional water surface elevation, m is the beach slope, L is a cross-shore length scale. The water surface elevation approaches the still water level far from the shoreline.

In order to simulate this situation in dimensional space a beach slope m of 0.02 and a length scale L of 20 m is chosen. The parameter ϵ is given by 0.2 in the simulation shown. The theory by Carrier and Greenspan (1958) predicts that a surging breaker results if the initial nondimensional depression is 0.23.

In this simulation the parameter s_0 in (18) is chosen to be unity so that the domain extends to infinity in the offshore direction. The depth threshold value at the shoreline D_{thresh} discussed in Section 3 is chosen as zero for this application. The simulation is carried out using 64 collocation points in the x-direction. A 16th order Shapiro filter is applied. Figure 5 (a) shows snapshots of the water surface elevation η as a function of offshore distance every 1.6 seconds, with $t = 0$ s corresponding to the initial depression of the water surface and the maximum rundown position, and $t = 19.2$ s corresponding to the maximum runup position. Figure 5 (b) shows the time series of the shoreline position. The numerical and analytical solutions are seen to agree to within visual resolution.

2D Runup

The second test case for the shoreline boundary condition involves solitary

wave runup on a bay with a sloping bottom. The test case geometry combines a curved shoreline with a sloping nearshore bathymetry that merges with a constant depth region offshore. This geometry is depicted in Figure 6. The still water surface is outlined with a single closed thick line above the bottom. The curved portion of the shoreline traces a period of a cosine curve. It is given by

$$\zeta(y, t = 0) = \zeta_0(y) = \frac{L}{\pi} \cos \frac{\pi y}{L} \tag{53}$$

where L is the half-width of the bay. The depth grid is given by

$$h = \begin{cases} h_0 - h_0 \frac{x - \frac{3L}{\pi}}{\zeta_0(y) - \frac{3L}{\pi}} & \text{for} \quad x \leq \frac{3L}{\pi} \\ h_0 & \text{for} \quad x > \frac{3L}{\pi} \end{cases} \tag{54}$$

where $h_0 = 0.4L/\pi$. The incoming wave is specified as a solitary wave. The dispersive parameter β given by $(h_0/L)^2$ is fixed at $(0.4/\pi)^2$ following the choice for h_0 and the wave height to offshore water depth ratio $\alpha = (H/h_0)$ of 0.02 is used. The incident wave on the constant depth region is then given by

$$\eta = \alpha h_0 \text{sech}^2 \left\{ \frac{\sqrt{gh_0}}{L} \chi \left(t + \frac{x}{\sqrt{gh_0(1+\alpha)}} \right) \right\}, \tag{55}$$

where

$$\chi = \sqrt{\frac{3\alpha}{4\beta}(1+\alpha)}. \tag{56}$$

Computations previously carried out by Zelt (1986) for this case show that breaking waves result if the wave height to water depth ratio is increased to 0.03. Zelt's (1986) calculations were carried out using a fully Lagrangian finite element model, the results show pronounced two dimensional runup.

In this simulation the parameter s_0 in (18) is chosen to be unity. Therefore, the domain extends to infinity in the offshore direction. The shoreline threshold depth D_{thresh} is chosen to be zero. The computations are carried out using 128 $\times$ 64 collocation points and a 16th order filter is applied in both horizontal directions.

Figure 7a shows normalized runup in the cross-shore direction as a function of the nondimensional time scale $t' = t\sqrt{gh_0}/L$ at different locations along the bay, where $y = 0$ denotes the midpoint of the bay and $y = \pm 1$ denote the boundaries in the longshore direction. Figure 7b shows the normalized maximum runup and rundown in the cross-shore direction as a function of longshore location. The present model is seen to compare well with results by Zelt (1986).

6.2 Absorbing-Generating Boundary

1D Absorption-Generation: A Group of Waves

The first test case for the offshore boundary condition involves the specification of a group of waves at the offshore boundary of a constant depth domain that is bounded onshore by a wall. The wave packet is expected to undergo a full reflection at the wall and travel back out of the domain at the offshore boundary. The packet is made up of sufficiently many waves so that a standing wave pattern will be formed. Eventually, no more incoming waves are present and the last waves reflect off the wall and leave the domain through the offshore boundary. Using this test, the error at the offshore boundary can be quantified since the wave height of the individual incident (H_{in}) and reflected (H_{out}) waves are expected to be the same although the shape of the waves is expected to change as they travel through the domain. The error can be quantified in the form of a reflection coefficient for simultaneous absorption-generation defined as

$$R_{ag} = \frac{|H_{in} - H_{out}|}{H_{in}}. \tag{57}$$

Once the theoretical amount of time for the wave packet to leave the domain has elapsed, any disturbances left in the domain are errors in the absorption process only as no generation is present at that time. Therefore, the reflection due to

only absorption can be quantified as

$$R_a = \frac{H_l}{H_{in}} \tag{58}$$

where H_l is the height of any leftover disturbance in the domain.

Figure 8 shows time series at the offshore boundary of the incident prescribed wave and the outgoing wave. The associated reflection coefficients, R_{ag} and R_a, are given in the caption of the figure and are about 0.06% and 0.02%, respectively. The reflection due to only absorption R_a is seen to be significantly lower than the reflection due to simultaneous absorption-generation R_{ag}. Since this was a consistent result of this and other similar test cases not shown here, results for only R_{ag} will be shown in the following test cases that focus on the effect of oblique incidence.

2D Absorption-Generation: Obliquely Incident Waves.

Keeping the same domain as in the previous test case, incoming waves are now specified at the offshore boundary at an angle to the offshore direction. Furthermore, the standing wave system that results from the reflection of such a wave from the wall is specified as an initial condition. The propagation and evolution of this system is then observed by continuing to specify the incoming wave and allowing the reflected wave to leave the domain. Several test cases involving different angles of incidence ranging from 0° to 67.5° are carried out. The reflection coefficient at the boundary R_{ag} is computed as before and is shown as a function of angle of incidence in Figure 9. It is seen to increase with angle of incidence but to remain below 1% for a wide range of angles.

7 Application: Subharmonic Edge Waves

We now consider whether the present model is intrinsically stable and non-dissipative enough to reproduce the analytically known properties of a certain nonlinear instability mechanism, in which subharmonic edge waves are excited by normally-incident, cleanly-reflected surface waves.

Guza and Davis (1974) showed that a monochromatic wave train, normally incident on a beach and strongly reflected, is unstable to edge wave perturbations, identifying a mechanism of edge wave generation through resonant interactions between the incident wave and the resulting edge waves. They also derived growth rates of the initially small edge wave perturbations and showed that the strongest resonance arises between the incident wave of period T_i and two mode zero edge waves of period $T_e = 2T_i$ traveling in opposite directions along the beach, forming a standing edge wave. This standing edge wave is hence a subharmonic of the incident wave. Guza and Bowen (1976) further analyzed this mechanism and identified three processes that may limit edge wave growth: further nonlinear edge wave-edge wave interactions leading to the radiation of edge wave energy into the far field, finite amplitude demodulation due to the fact that the natural frequency of the edge wave σ_f increases with amplitude and eventually detunes such that the forcing frequency ceases to lie within the resonant bandwidth, and viscosity.

Using nonlinear perturbation analysis, Guza and Bowen (1976) showed that radiation and detuning are of comparable importance in limiting edge wave growth and that viscosity is relatively unimportant, once edge wave growth is initiated. In their analysis, the lowest order potential is described as the sum of the normally incident wave at frequency 2σ and the standing edge wave at the

subharmonic frequency σ such that

$$\phi_0 = \phi_i + \phi_e \tag{59}$$

where

$$\begin{aligned} \phi_i &= \frac{a_i g}{2\sigma} J_0(\chi) \sin 2\sigma t \quad \text{where} \quad \chi^2 = \frac{4(2\sigma)^2 x}{gm} \\ \phi_e &= \frac{a_e g}{\sigma} e^{-\lambda x} \cos \lambda y \cos(\sigma t + \theta), \end{aligned} \tag{60}$$

where m is the beach slope, λ is the edge wave wavenumber. The variable θ is the phase difference between the incident and edge waves and a_i and a_e are the amplitudes of the water surface elevations of the lowest order incident and edge wave, respectively, at the still water shoreline.

The theory by Guza and Bowen (1976) predicts that the frequency band within which edge waves will grow for a given wavelength in the absence of viscosity is centered on $\sigma_0 = gm\lambda$, where the initial growth rate is maximum, and has the bandwidth

$$(1 - 0.0338\epsilon_i)\sigma_f \leq \sigma \leq (1 + 0.0338\epsilon_i)\sigma_f. \tag{61}$$

The parameter ϵ_i is a measure of the nonlinearity of the incident wave and is given by

$$\epsilon_i = \frac{a_i(2\sigma)^2}{gm^2}. \tag{62}$$

Perturbation analysis predicts the natural edge wave frequency σ_f as

$$\sigma_f = (1 + 0.055\epsilon_e^2)\sigma_0. \tag{63}$$

where

$$\epsilon_e = \frac{a_e \sigma^2}{gm^2}, \tag{64}$$

is a measure of the nonlinearity of the edge wave.

Their results further indicate an upper limit on the possible maximum edge wave amplitude for a given frequency σ due to the effects of radiation and detuning in the absence of viscosity. This upper limit is given by

$$\epsilon_e = 0.767\sqrt{\epsilon_i} \tag{65}$$

This edge wave amplitude occurs when the forced edge wave has frequency σ_f given by (63) as $(1 + 0.0324\epsilon_i)\sigma_0$, as stated by Rockliff (1978). The phase of the edge wave in relation to the incoming wave can also be determined. The maximum nondimensional edge wave amplitudes and the phase differences are given in Figure 10 as a function of a nondimensional detuning parameter Δ. The actual edge wave frequency is given by

$$\sigma = (1 + 0.0338\Delta\epsilon_i)\sigma_0. \tag{66}$$

The maximum response occurs at $\Delta = 0.96$.

Existing laboratory experiments (Bowen and Inman, 1971; Guza and Inman, 1975) confirm that edge wave amplitudes substantially larger than the incoming wave amplitude at the shoreline occur when the incoming wave is strongly reflected by the beach. However, the subharmonic resonance ceases when the wave breaks cleanly, which occurs at $\epsilon_i \cong 2$ (Guza and Inman, 1975).

The numerical model of the nonlinear shallow water equations described in Sections 3-6 is expected to reproduce the theoretically predicted and experimentally observed phenomenon of the generation of subharmonic edge waves and their growth to finite amplitude. For a simulation, a beach slope of 0.1 is chosen, the longshore width L_y of the domain is chosen to be $(2\pi/\lambda)$, where λ is determined such that the natural frequency of a small amplitude edge wave is $\sigma_0 = 2\pi/20$ rad/sec. The amplitude of the incident wave is specified as $A = 0.01$ m at the offshore boundary located at $x = 100$ m. Since the low-

est order water surface elevation of the incident wave is given by

$$\eta_i = a_i J_0(\chi) \cos 2\sigma t, \tag{67}$$

a_i can be determined to be 0.091 m. Furthermore, an initial perturbation at the subharmonic edge wave wavenumber is introduced by specifying the initial water surface elevation to be

$$\eta_e(x, y, 0) = a_e e^{-\lambda x} \cos \lambda y. \tag{68}$$

The initial amplitude $a_e = O(10^{-3})$ and $u = v = 0$ are also specified and the growth of the edge wave amplitude a_e is observed. Edge waves of different periods can be forced by varying the period of the incoming wave. The physical domain is modeled using 64×32 collocation points. An 8th order Shapiro filter is applied in both horizontal directions, and the depth threshold value at the shoreline D_{thresh} discussed in Section 3 is chosen as 1 mm.

Since a complete time series is not available at the still water shoreline as it becomes dry during the rundown period, time series at $x = 6$ m are used to determine the equilibrium amplitude of the edge wave. Figure 11 shows the theoretical maximum edge wave amplitude at $x = 6$ m as a function of the nondimensional detuning parameter Δ.

The computed maximum edge wave amplitude is found for comparison with theory by isolating the linear edge wave component at the frequency $f = \sigma/2\pi$ by bandpassing the computed time series of the water surface elevation at $(x, y) = (6\text{m}, 0\text{m})$ using a bandwidth of 0.02 Hz. Furthermore, the phase relation between the bandpassed edge wave and the lowest order incident wave given in (67) can also be determined by observing the time lag between zero-upcrossings of the incident and edge wave.

Time series for edge waves corresponding to a number of Δ values ranging from -1.06 to 1.04 have been simulated and shown in Figure 12. The time series

are recorded at $y = 0$ where maximum runup of the standing edge wave occurs. The figure shows that the equilibrium amplitude is reached most rapidly for $\Delta = 0$, corresponding to an edge wave at the linear natural period of $T_e = 20$ sec, where the initial growth rate of the instability is highest. It can be noted that the maximum amplitude is reached later for cases corresponding to higher $|\Delta|$ values. This is consistent with theory since the initial growth rates decrease with increasing $|\Delta|$. The instability ceases to exist altogether for $|\Delta| > 1$.

Figure 11 also shows the nondimensional maximum edge wave amplitude for model results for the cases seen in Figure 12. It can be observed that the low and high frequency cut-offs of the unstable motion below and above which edge wave perturbations are stable are predicted. Also shown are the phase differences between the edge wave and the incoming wave predicted by theory and numerical computations. It is seen that the phase lag increases with increasing Δ.

8 Summary and Conclusions

A model of the nonlinear shallow water equations has been developed with the objective of studying low frequency motions in the surf and swash zones. A high order time integration scheme has been used in conjunction with spectral collocation for the calculation of spatial derivatives. Two dimensional shoreline runup is modeled using a Eulerian shoreline model in conjunction with a moving grid. This method compares favorably to analytical and numerical results for both one-dimensional and two-dimensional shoreline runup. An absorbing-generating boundary condition is used at the offshore boundary. It is shown that errors (in the form of partially reflected waves) remain small for a wide range of incident angles.

The model is used to predict the growth of subharmonic edge waves to finite amplitude. This application is physically representative of the complexity

of motions in the surf and swash zones since onshore and longshore directed motions coexist and interact to create a wave field with significant two dimensional shoreline runup. It also constitutes a severe and physically relevant test of the model. Since high amplitude edge waves cause significant two dimensional shoreline runup, an accurate shoreline treatment is important. Since the edge wave amplitudes are limited by the loss of energy to waves radiating offshore, the absorbing boundary condition is essential. Furthermore, since the maximum edge wave amplitude is reached at large time scales with respect to the periods involved, low dispersion and dissipation errors are desired.

The growth of subharmonic edge waves to finite amplitude is successfully simulated. The equilibrium edge wave amplitudes and phases are predicted with satisfactory agreement to weakly nonlinear theory. Neutral stability characteristics of the motion are also reproduced since a high frequency and low frequency cut-off are predicted and edge waves with frequencies beyond the unstable frequency band are observed to be stable. Since the predicted motion results from a physical instability of the basic state, the predicted low and high frequency cut-off points demonstrate that the model reproduces physical instabilities while remaining numerically stable.

It can be concluded that the developed numerical model is suitable for the further study of complex surf zone phenomena such as longshore and cross-shore directed currents, edge waves and shear waves and the nonlinear interactions between them. Preliminary results on long time evolution of shear instabilities of longshore currents may be found in Özkan and Kirby (1995) and Özkan-Haller and Kirby (1996). The model is also being extended at present to include the effects of time-varying short wave forcing, applied through the action of radiation stress terms.

Acknowledgments. This research is sponsored by the Office of Naval Research, Coastal Sciences Program under Grant N00014-94-1-0214.

References

Abbott, M.B. (1979). *Computational Hydraulics. Elements of the Theory of Free Surface Flows.* Pitman Publishing.

Allen, J.S., P.A. Newberger and R.A. Holman (1996). "Nonlinear shear instabilities of alongshore currents on plane beaches." *J. Fluid Mech.*, **310**, 181-213.

Bowen, A.J. and D.L. Inman (1971). "Edge waves and crescentic bars." *J. Geophys. Res.*, **76**, 8662-8671.

Bowen, A.J. and R.A. Holman (1989). "Shear instabilities of the mean longshore current. 1. Theory" *J. Geophys. Res.*, **94**, 18023-18030.

Boyd, J.P. (1988). *Chebyshev & Fourier Spectral Methods.* Springer-Verlag, New York, N.Y.

Canuto, C. M.Y. Hussaini, A. Quarteroni and T.A. Zang (1987). *Spectral Methods in Fluid Dynamics.* Springer-Verlag, New York, N.Y.

Carrier, G.F. and H.P. Greenspan (1958). "Water waves of finite amplitude on a sloping beach." *J. Fluid Mech.*, **4**, 97-109.

Dalrymple R.A., J.T. Kirby and P.A. Martin (1994). "Spectral methods for forward-propagating water waves in conformally-mapped channels." *Appl. Ocean Res.*, **16**, 249-266.

Falqués, A. and V. Iranzo (1992). "Edge waves on a longshore shear flow." *Phys. Fluids A*, **4**, 2169-2190.

Gopalakrishnan, T.C. and C.C. Tung (1983). "Numerical analysis of a moving boundary problem in coastal hydrodynamics." *Intl. J. Numer. Meth. Fluids*, **3**, 179-200.

Gottlieb, D., M. Gunzburger and E. Turkel (1982). "On numerical boundary treatments for hyperbolic systems." *SIAM J. Numer. Anal.*, **19**, 671-697.

Guza, R.T. and A.J. Bowen (1976). "Finite amplitude edge waves." *J. Marine Res.*, **34**, 269-293.

Guza, R.T. and R.E. Davis (1974). "Excitation of edge waves by waves incident on a beach." *J. Geophys. Res.*, **79**, 1285-1291.

Guza, R.T. and D.L. Inman (1975). "Edge waves and beach cusps." *J. Geophys. Res.*, **80**, 2997-3012.

Liu, P.L.-F., Y.-S. Cho, M.J. Briggs, U. Kanoglu and C.E. Synolakis (1995). "Runup of solitary waves on circular island." *J. Fluid Mech.*, **302**, 259-285.

Lynch, D.R. and W.G. Gray (1980). "Finite element simulation of flow in deforming regions." *J. Comp. Phys.*, bf 36, 135-153.

Oltman-Shay, J., P.A. Howd and W.A. Birkemeier (1989). "Shear instabilities of the mean longshore current. 2. Field observations." *J. Geophys. Res.*, **94**, 18031-18042.

Özkan, H.T. and Kirby, J.T. (1995). "Finite amplitude shear wave instabilities." *Proc. Coastal Dynamics 1995*, Gdansk, Poland, 465-476.

Özkan-Haller, H.T. and Kirby, J.T. (1996). "Numerical study of low frequency surf zone motions." *Proc. 25th Intl. Conf. Coastal Eng.*, Orlando, Florida.

Panchang, V.G. amd D.A. Kopriva (1989). "Solution of two-dimensional water-wave propagation problems by Chebyshev collocation." *Mathl. Comput. Modelling*, **12**, 625-640.

Pedersen, G. and B. Gjevik (1983). "Run-up of solitary waves." *J. Fluid Mech.*, **135**, 283-299.

Rockliff, N. (1978). "Finite amplitude effects of free and forced edge waves." *Proc. Camb. Phil. Soc.*, **83**, 463-479.

Shapiro, R. (1970). "Smoothing, filtering and boundary effects." *Reviews of Geophys. and Space Phys.*, **8**, 359-387.

Van Dongeren, A.R., F.E. Sancho, I.A. Svendsen and U. Putrevu (1994). "SHORE-CIRC: A quasi 3-D nearshore model." *Proc. 24th Intl. Conf. Coastal Eng.*, Kobe, 2741-2754.

Verboom, G.K. and A. Slob (1984). "Weakly-reflective boundary conditions for two-dimensional shallow water flow problems." *Adv. Water Resources*, **7**, 192-197.

Zelt, J.A. (1986). "Tsunamis: The response of harbours with sloping boundaries to long wave excitation." Report No. KH-R-47, California Institute of Technology, Pasadena, California.

Zelt, J.A. and F. Raichlen (1990). "A Lagrangian model for wave-induced harbour oscillations." *J. Fluid Mech.*, **213**, 203-225.

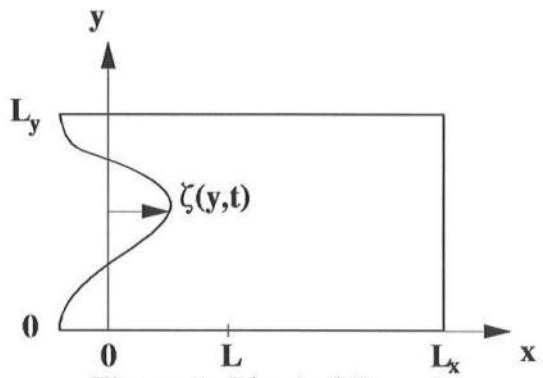

Figure 1: Physical Domain

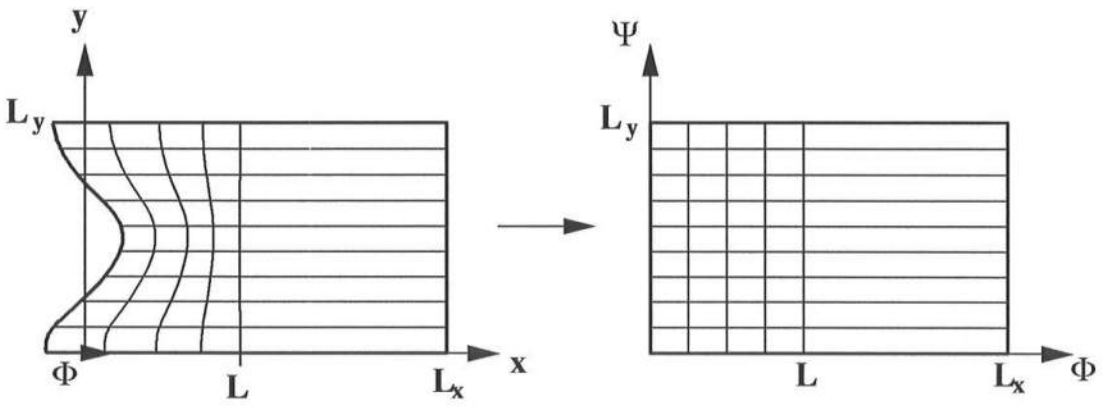

Figure 2: Shoreline Boundary Condition: Transformation from the physical to the intermediate domain

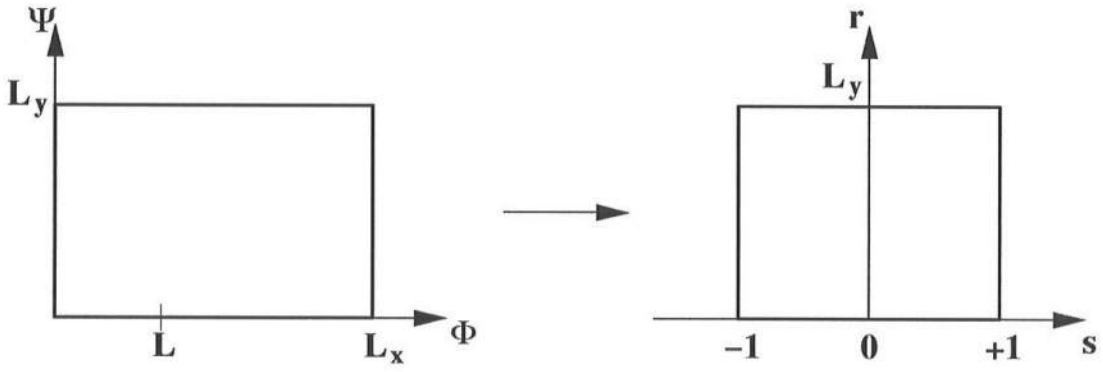

Figure 3: Transformation from the intermediate to the computational domain

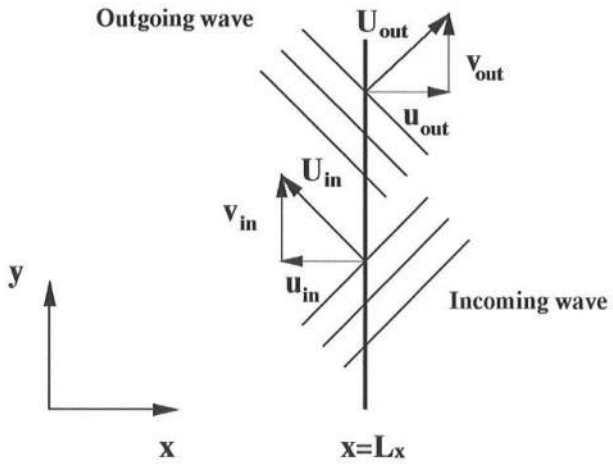

Figure 4: Sketch of the offshore boundary

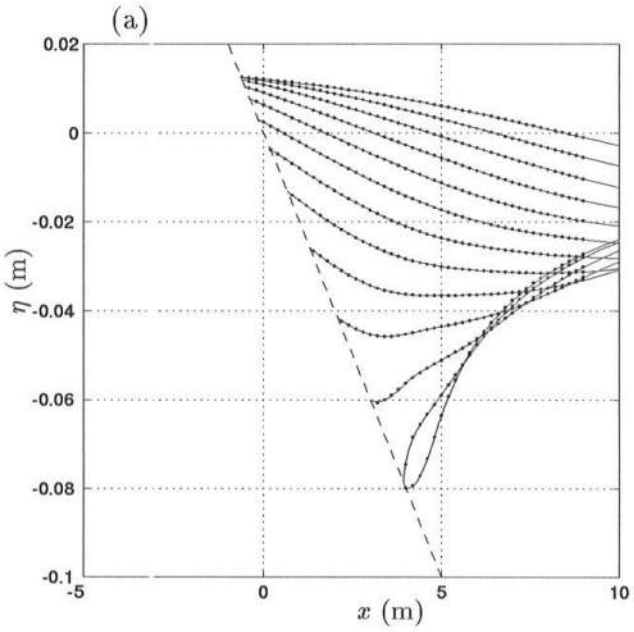

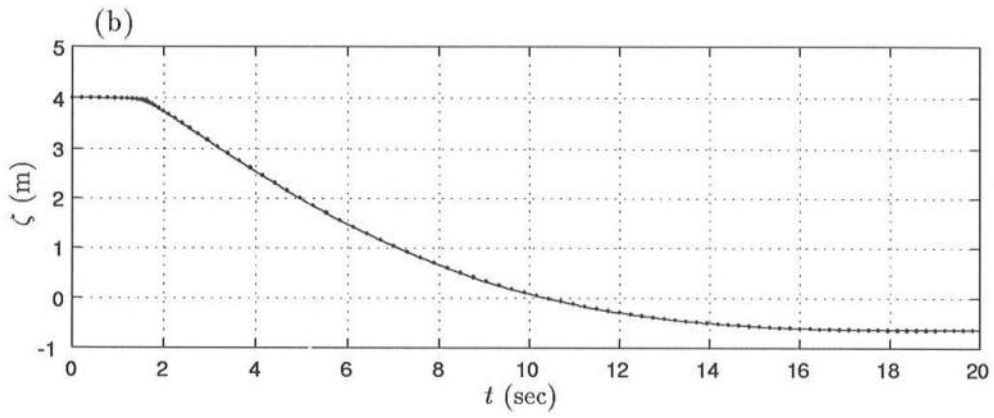

Figure 5: Runup in 1D: (a) Snapshots with $\Delta t = 1.6$ sec of η versus x. (b) Time series of shoreline position. Exact solution (· · · · · ·), present model (———).

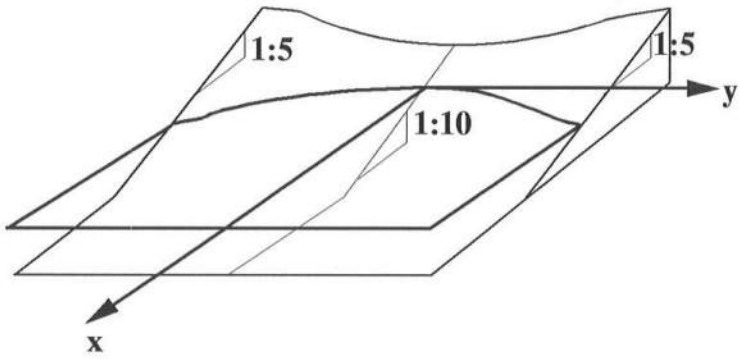

Figure 6: Bathymetry of the 2D runup test case.

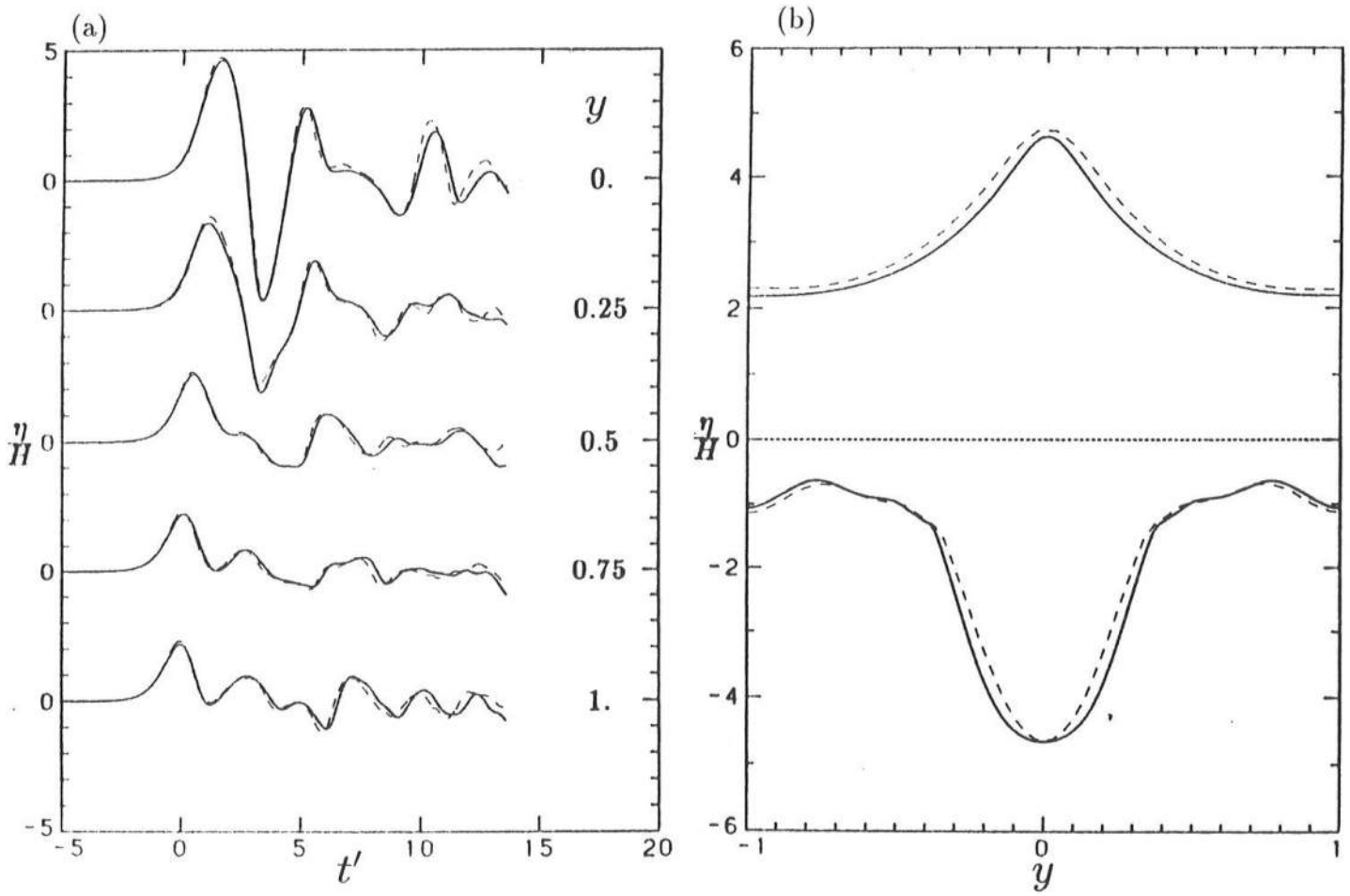

Figure 7: (a) Runup in 2D: Time series of runup along y. (b) Maximum runup and rundown. Zelt (———), present model (– – –).

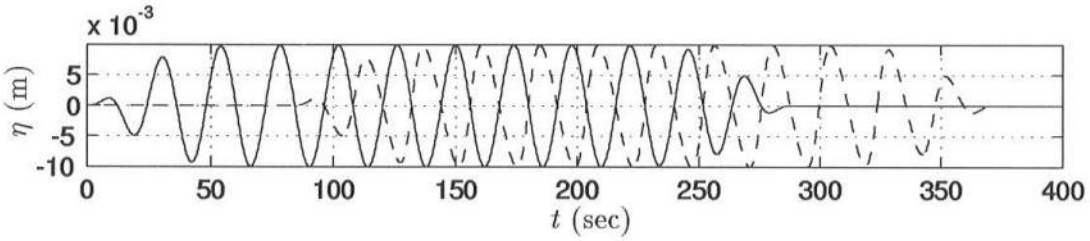

Figure 8: Simultaneous absorption-generation: Incoming wave (———) and outgoing wave (– – –). $R_{ag} = 6.3 \times 10^{-4}$, $R_a = 1.9 \times 10^{-4}$

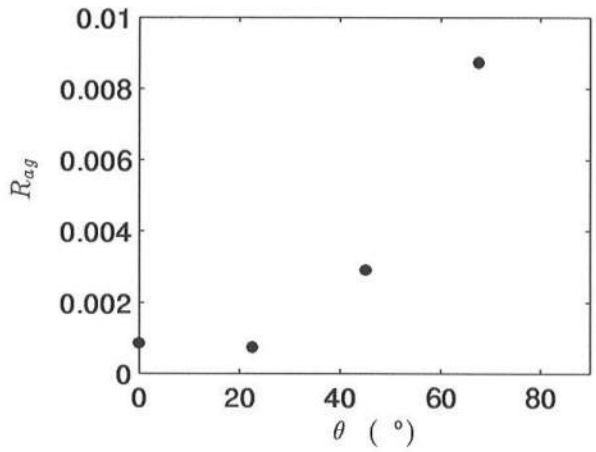

Figure 9: Simultaneous absorption-generation: Reflection as a function of incident angle θ.

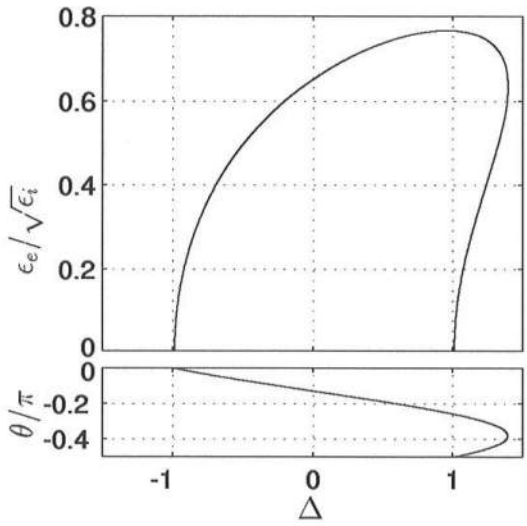

Figure 10: Equilibrium nondimensional amplitude of a subharmonic edge wave and its phase θ in relation to the incoming wave as a function of edge wave frequency detuning.

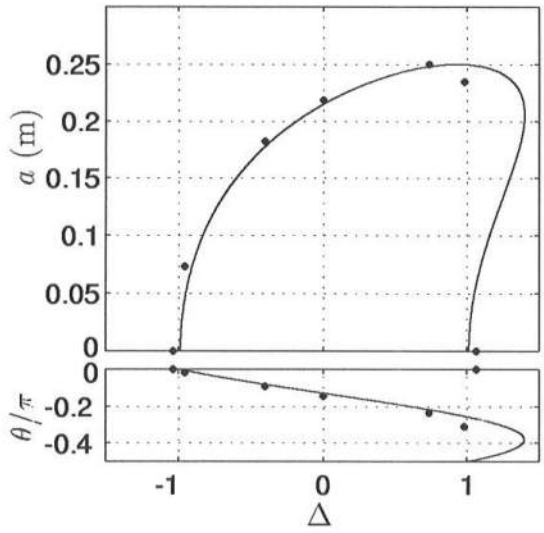

Figure 11: Equilibrium amplitude of a subharmonic edge wave at $x = 6$ m and its phase θ in relation to the incoming wave as a function of edge wave frequency detuning. Perturbation theory (———), model (•).

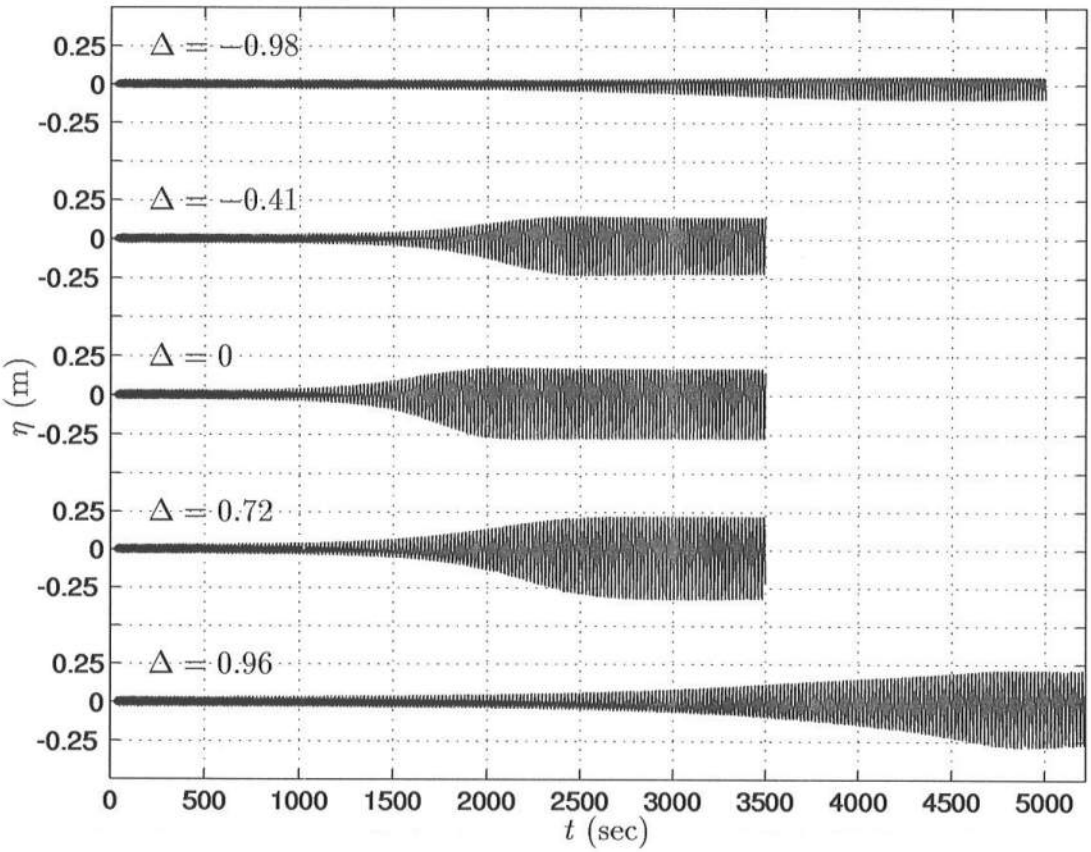

Figure 12: Water surface elevation η at $(x, y) = (6, 0)$ m for various Δ values